Chapter 14
The Stability of Non-linear Power Systems

Kaihua Xi, Johan L. A. Dubbeldam, Feng Gao, Hai Xiang Lin, and Jan H. van Schuppen

Abstract The power system is one of the most complicated man-made non-linear systems which plays an important role for human being since it was first made in the 19th century. In the past decade, the integration of renewable power sources such as wind energy and solar energy has increased rapidly due to their sustainability. However, these energy sources are weather dependent which cannot be controlled or even predicted precisely. A challenge brought by this transition to renewable power generation is the uncertain fluctuations that negatively affects the stability of the power system, which leads to the important problem: how to improve by control the stability of the system such that it remains stable when subjected to considerable fluctuations in the energy supply? Hence, research is needed into the stability metrics of the non-linear power system and control strategies for the stability improvement. In this chapter, we describe the linear and non-linear stability analysis of power systems and summarize the corresponding control strategies for stability improvement.

K. Xi (✉)
School of Mathematics, Shandong University, Jinan 250100, Shandong, China
e-mail: kxi@sdu.edu.cn

F. Gao
School of Electrical Engineering, Shandong University, Jinan 250061, Shandong, China
e-mail: fgao@sdu.edu.cn

J. L. A. Dubbeldam · H. X. Lin · J. H. van Schuppen
Delft Institute of Applied Mathematics, Delft University of Technology, Van Mourik Broekmanweg 6, 2628 XE Delft, The Netherlands
e-mail: J.L.A.Dubbeldam@tudelft.nl

H. X. Lin
e-mail: H.X.Lin@tudelft.nl

J. H. van Schuppen
e-mail: J.H.vanschuppen@tudelft.nl

A. K. Abramian et al. (eds.), *Nonlinear Dynamics of Discrete and Continuous Systems*, Advanced Structured Materials 139,
https://doi.org/10.1007/978-3-030-53006-8_14

14.1 Introduction

In order to decrease the CO_2 emissions from the traditional fossil fuel power plants, there are more and more wind farms and Photo Voltaic (PV) farms established on the generation side and rooftop solar PV panels installed at houses of consumers on the distribution side almost all over the world in the past decade. The rapid increase of the weather dependent power energy, which is also called variable renewable energy, brings several challenges to the power system. It is well known that these renewable power generation depends on the weather which cannot be controlled or even accurately predicted. In this case, unlike the traditional power system where the uncertainties usually come from the consumer side only, the uncertainties now come from both the generation and the load side and thus will be harder to manage. These fluctuations do not only deteriorate the quality of power supply, but also decrease the power system stability [28].

Since power systems rely on the synchronous machines (e.g., rotor-generators driven by steam or gas turbines) for power generation, a requirement for normal system operation is that all the synchronous machines remain in synchronization. The ability of a power system to maintain the synchronization when subjected to severe transient disturbance such as short-circuit of transmission lines, loss of generation, is called *transient stability* [1, 10, 18, 22, 51], which we will also refer to as synchronization stability in this chapter. The synchronous state is actually an *equilibrium point* of the system, which has been widely studied in the field of complex network [25, 41, 47]. Synchronization stability has been studied mainly by linearizing about a stable equilibrium [2, 12, 32, 34, 39]. The framework developed by Pecora et al. has greatly facilitated these computations. However, as fluctuations induced by changing weather can have enormous impact, a linearization approach will often not be sufficient. From the perspective of non-linear systems, this stability measures the ability that the state stays in the basin of attraction after disturbances. This stability is influenced by the nonlinearity of the power system. The basin of attraction (also called the *stability region*) of a nonlinear system is defined as the set of the initial states of the trajectories which converge to the equilibrium as the time goes to infinity [19, 37]. For a nonlinear system with a small basin of attraction, the trajectory usually has a small escape time from the region when subjected to disturbances. *Stability margin* is another definition corresponding to the non-linear stability, which measures the distance from a stable state to the state of losing synchronization [10, 17, 51]. The larger the stability margin, the more stable is the power system against disturbances.

For a power system, the non-linear stability depends on the severity of the disturbance. Renewable energy such as wind power and solar power is often strongly affected by the weather and consequently causes power fluctuations and frequency fluctuations of a large-scale power system. These continuous fluctuations of the frequency may further lead the system to lose the synchronization. In order to further increase the integration of the renewable energy, the problem of *increasing the synchronization stability to avoid losing frequency synchronization caused by various*

disturbances is receiving more and more attention. It is obvious that the decrease of the strength of the disturbance can effectively increase the stability. The strategies on how to suppress these disturbances is not the focus of the chapter. We pay attention to the possible strategies for improving the stability by changing the power system itself, which consists of synchronous power generators, power transmission lines and loads.

Control of power systems can enhance the system stability. The control objectives for control of a power system include to deliver electric power to customers of the network operator, to maintain the stability of the power system, preferably in the domain of attraction of the current steady state, and to minimize the cost of the operation of the power system. In practice, the power transmission in the first control objective depends on the location of the power generation and loads, the network topology and the transmission line capacity. The latter two control objectives are separated for frequency control into primary, secondary and tertiary frequency control, respectively, see [22, 53]. The primary control which also called droop control keeps the synchronization of the frequency at a value which may deviate from the nominal value. The secondary control the synchronized frequency to the nominal frequency and the tertiary control determine the set point stabilized by the primary and secondary control. The secondary control and the tertiary control jointly determine the set point of the power system. In addition, the secondary control affects the dynamics.

The control objective of maintaining the state of the system within a domain of attraction of a steady state motivates research to explore ways to characterize the stability region, the boundary of the domain of attraction and the stability margin [11, 58]. For a power system with control, the stability depends on factors such as

(i) the topology of the network, which can be changed by adding new lines and nodes to the network or configuring the capacity of the lines,
(ii) the inertia of the synchronous machines, which may be changed by placing or removing virtual inertia to the nodes in the network,
(iii) the damping coefficients of the synchronous machine, which includes the droop control gain parameter that can be configured in droop control [22],
(iv) and power generation and load, which can be controlled by changing the mechanical power generation or switching on or off the power consumption.

To accomplish the control objective of keeping the system stability, these four factors can be changed based on characteristics of the stability region. The first step for the stability improvement is to find a metric for the stability, which can point to those factors that are best changed. The need for improving the stability of a power systems motivates research into the mathematics of stability analysis of power systems.

In this chapter, we focus on the improvement of the stability of power systems. We give a survey on the recent development of the stability analysis and summarize the potential stability metrics for the stability and corresponding strategies for the stability improvement. The chapter is organized as follows. Section 14.2 introduces the model of the power systems. Section 14.3 discusses the necessary condition for

the existence of synchronization state. The linear stability and non-linear stability of the synchronization state are described in Sects. 14.4 and 14.5 respectively. We conclude the chapter in Sect. 14.6.

14.2 The Model of Power Systems

There are three main components in power systems, namely power generators, transmission network, and loads. We consider the power system described by a graph $\mathcal{G} = (\mathcal{V}, \mathcal{E})$ with nodes $\mathcal{V}$ and edges $\mathcal{E} \subseteq \mathcal{V} \times \mathcal{V}$ where a node represents a bus and edge (i, j) represents the direct transmission line connection between node i and node j. Each bus is locally connected to either energy sources, or energy loads, or to both. We denote the number of nodes in the network by n.

We focus on the power system with lossless transmission lines, of which the dynamics can be equivalently described by the following swing equations [4, 9, 31],

$$\dot{\delta}_i = \omega_i, \ i \in \mathcal{V}, \tag{14.1a}$$

$$M_i \dot{\omega}_i = P_i - D_i \omega_i - \sum_{j \in \mathcal{V}} B_{ij} \sin(\delta_i - \delta_j), \ i \in \mathcal{V}, \tag{14.1b}$$

where δ_i is the phase angle at node i, ω_i is the frequency deviation from the nominal frequency, e.g., 50 or 60 Hz, $M_i > 0$ is the moment inertia of the machine, P_i is the power supplied by synchronous machines or by renewable energy sources if $P_i > 0$, and is power load if $P_i < 0$, $D_i > 0$ is the damping coefficient including droop control gain parameter, $B_{ij} = \hat{B}_{ij} V_i V_j$ which can be viewed as the weight of the edges in the graph $\mathcal{G}$. Since the control of the voltage and of the frequency can be decoupled when the transmission lines are lossless [45], we do not model the dynamics of the voltages and assume the voltage of each bus is a constant which can be derived from power flow calculation [33, 42].

Throughout the discussion of this chapter, we assume the network is undirected and connected. The Laplacian matrix of the network is in the form

$$L_n = \begin{pmatrix} \sum_{j=1}^n B_{1j} & -B_{12} & \dots & -B_{1n} \\ -B_{21} & \sum_{j=1}^n B_{2j} & \dots & -B_{2n} \\ \vdots & \vdots & \ddots & \vdots \\ -B_{n1} & -B_{n2} & \dots & \sum_{j=1}^n B_{nj} \end{pmatrix} \tag{14.2}$$

Because the line weight $B_i j$ for all $(i, j) \in \mathcal{E}$ are positive, L_n is non-negative definite. The eigenvalues of $L_n \in \mathbb{R}^{n \times n}$ are denoted by $0 < \sigma_2 \leq \cdots \leq \sigma_n$. Herein, the second smallest eigenvalue σ_2 measures the connectivity of the network [50].

It has been demonstrated in [43, 44] that frequency droop controlled Micro-Grids which have some sort of energy storage and lossless transmission lines can also be modeled by second-order swing equations (14.1). Some other models are also applied for the synchronization stability analysis of power networks, see [36] for details of the comparison of these models.

By selecting one node as infinite bus with constant phase and the other one as a synchronous generator in a two-node network, the following *Single Machine Infinite Bus* (SMIB) model can be obtained,

$$\dot{\delta} = \omega, \tag{14.3a}$$

$$M\dot{\omega} = P - D\omega - B\sin\delta, \tag{14.3b}$$

which can be directly derived from (14.1). Here P and B are the transmitted power and the line capacity respectively, the voltages are also assumed constant, δ is the angle difference between the synchronous machine and the infinite bus, which should be kept in a small range in order to stay in the synchronization state. This requires $\omega = 0$ and $P = B\sin\delta$ at the synchronized state. The diagram of this SMIB model is shown in Fig. 14.1.

The modeling of fluctuations affecting a power system are discussed next, because such fluctuations strongly motivate current research in stability analysis and control of power systems.

In practice, continuous fluctuations act 24 h a day, though their intensity varies during the day and depend on the weather and on human behavior. The energy loads fluctuate all the time due to consumers switching on electricity devices. The power generation of the synchronous generators are operated to balance these fluctuations and keep the stability of the power system.

Weather dependent power sources as wind turbines, wind parks, and the sun via photo-voltaic panels, generate power with large fluctuations. The wind power produced varies with the intensities of the wind force, the solar power produced varies with the sun intensities received on earth and with the cloud covers between the sun and the PV panel. The strength of these fluctuations are much stronger than those in the traditional power system, which bring great challenges to the operation of the power systems. Modeling of the fluctuations and procedures of system identification may help to obtain realistic models for control of power systems to suppress the fluctuations. Effective suppression of the fluctuations are important for the synchronous stability of the power systems.

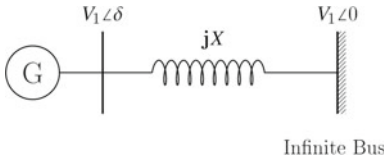

Fig. 14.1 The SMIB model

Abrupt changes in the transmission network may occur, which could cause serious blackouts. These events have happened more frequently in the past decade than before. Examples of such abrupt changes are the breakage of power lines, for example due to freezing rain on the lines, break down of part of a power plant with synchronous machines, or instability of the power network due to a network node experiencing a relatively large power disturbance. For such abrupt changes there are special control procedures, like islanding of the power network, control of each power network island, and later return to the normal state by joining the power network islands. These procedures are not further discussed in this chapter. The focus of this chapter is on analysis of power system stability and on control for the improvement of power system stability.

14.3 The Synchronous State

The stability of a nonlinear system usually refers to the ability of the system to stay in the basin of attraction of a synchronous state. In this section, the focus is on the existence of the synchronous state of the power system.

The equilibrium point of the system (14.1) is referred to as the *synchronous state* defined as follows.

Definition 14.1 Assuming that power generation and loads are constant, the synchronous state of the system satisfies for all $i \in \mathcal{V}$

$$\omega_i = \omega_{syn}, \tag{14.4a}$$

$$\dot{\omega}_i = 0, \tag{14.4b}$$

$$\delta_i = \omega_{syn} t + \delta_i^*, \tag{14.4c}$$

$$\dot{\delta}_i = \omega_{syn}, \tag{14.4d}$$

where $\omega_{syn} \in \mathbb{R}$ is the synchronized frequency deviation, δ_i^* is the phase angle of node i at the steady state. In the synchronous state, all the phase distances $|\delta_i - \delta_j| = |\delta_i^* - \delta_j^*|$ are constant.

The terminology *phase locking* and *phase cohesiveness* are also used to describe this synchronization state of frequency [15]. In particular, the phase locking state with $|\delta_i^* - \delta_j^*| = 0$ for $i, j = 1, \ldots, n$, is called *phase synchronized* state. In practice, the synchronous state does not exist for the power system due to the continuously fluctuating power loads. However, it is practical to assume the power loads are constant on small time-scales which lead to a synchronous state.

By summing all the equations for $i = 1, \ldots, n$, the explicit formula of the synchronized frequency ω_{syn} can be obtained as follows

$$\omega_{syn} = \frac{\sum_{i=1}^{n} P_i}{\sum_{i=1}^{n} D_i}, \tag{14.5}$$

where $\sum_{i=1}^{n} P_i$ is referred to as the *power imbalance*. It can be obtained that if the power imbalance is zero, the synchronized frequency deviation is zero. The restoration of the frequency deviation to zero is the task of secondary frequency control, see [16, 20, 53, 54, 56].

14.3.1 Existence of the Synchronous State

For the SMIB model, the equilibrium point satisfies

$$\omega = 0, \quad \sin \delta^* = \frac{P}{B}. \tag{14.6}$$

at which the phase angle difference between the machine and infinite bus is δ^*. It is obvious that if $B < P$, this equilibrium point does not exist and the system converges to a *non-synchronous limit cycle* which can be characterized by

$$\omega_{ns} \approx \frac{P}{D} + \frac{DB}{P} \cos\left(\frac{P}{D} t\right) \tag{14.7}$$

when $|P|/D^2 \gg 1$ and $P^2/D^2 \gg B$, see [31]. For this SMIB model, the *critical line capacity* is $K_c = P$, which is the power that has to be transmitted to the load. This critical line capacity is also called *critical coupling* [14], which is defined as the smallest line capacity for the existence of an equilibrium point. If $B > K_c$, it is obvious that in a period of sin function there are two equilibrium points which satisfy (14.6), However, it is far more complex to obtain an explicit formula of the critical capacity for the power system (14.1) than for the SMIB model. It is obvious that the existence of the synchronous state depends on the power injection (load), the topology of the network and the line capacities. Hence, the critical line capacity depends on the power injection (load) and the network topology.

Due to the importance of the synchronization in complex network, the Kuramoto model is widely studied for the condition of the synchronization. The *first-order non-uniform Kuramoto model* is as follows

$$\dot{\delta}_i = \omega_i - K \sum_{j=1}^{n} a_{ij} \sin(\delta_i - \delta_j), \ i = 1, \ldots, n. \tag{14.8}$$

where $a_{ij} = 1$ if node i and j is connected, otherwise $a_{ij} = 0$. Note that the model (14.1) is also referred to as *non-uniform second-order Kuramoto model*. The corresponding Laplacian matrix is denoted by $\boldsymbol{L}_a$. Here ω_i has a different meaning from the one in the power system (14.1), which denotes a force to the oscillator i. In literature, the critical line capacity K_c has been widely applied to the study of the impact of the parameter of the system on the existence of the synchronous state. If the critical coupling strength $K > K_c$, it satisfies $\dot{\theta}_i = \omega_s$ for all the nodes in the

network where $\omega_s = \sum_i^n \omega_i/n$, which can be obtained by summing all the equation in (14.8). For completed network with $a_{ij} = 1$ for $i, j = 1, \ldots, n$, the upper bound and lower bound of K_c can be obtained explicitly [15]. For a general network, the lower bound of K_c can be obtained from the necessary condition or the sufficient condition for the existence of the synchronous state of (14.8), see [15]. The critical coupling strength depends on the distribution of ω_i and the network topology, the synchronization can improved via decreasing K_c by changing the topology and the distribution of the frequency ω_i. In order to connect these conditions to the power systems, Dörfler and Bullo [14] have proven the equivalence of the synchronization of the power network (14.1) and the Kuramoto network (14.8). With this equivalence, the existence condition of the synchronous state for the power system (14.1) can be deduced from those of the Kuramoto model (14.8).

Remark 14.1 With the lower bound of K_c as a stability metric, an optimization framework can be formed with the controllable factors, i.e., the network topology and the power generation and loads, as decision variables. Because the inertia and the damping coefficient have no influence on the synchronous state when $\omega_{syn} = 0$, this metric cannot be applied for the improvement of the stability by controlling the virtual inertia and damping coefficients.

The stability of the synchronous state can be determined by the Lyapunov method, which will be further described in Sect. 14.4. In principle there may be more than one stable synchronous state [13, 27, 29, 38, 40, 55] due to cycles in the network.

For a cyclic power network with alternating nodes of loads and generators as shown in Fig. 14.2. There are even number of nodes in the network and the power injection $P_i = -2P$ for even nodes and $P_i = 2P$ for odd nodes. This alternating distribution of power leads to $\sum_{i=1}^n P_i = 0$. The model of this network can be deduced from (14.1) as

$$\dot{\delta}_i = \omega_i, \tag{14.9a}$$

$$\dot{\omega}_i = P_i - D\omega_i - B[\sin(\delta_i - \delta_{i+1}) + \sin(\delta_i - \delta_{i-1})]. \tag{14.9b}$$

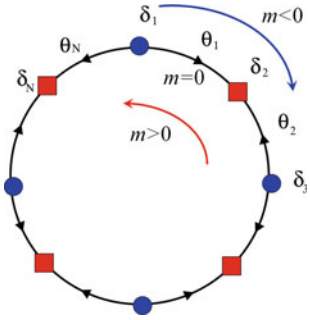

Fig. 14.2 A cyclic network with alternating consumer and generator nodes. Circle nodes are generators and square nodes are consumers. There may be stable equilibria with the power transported around the cycle clockwise with $m < 0$ and counterclockwise with $m > 0$

Denote the phase differences between neighbors by $\theta_1 = \delta_1 - \delta_n \pmod{2\pi}$ and $\theta_{i+1} = \delta_{i+1} - \delta_i \pmod{2\pi}$. The equilibria of this ring network are given by $\theta_i = \theta_1$ for odd i, and $\theta_i = \theta_2$ for even i, where

$$\theta_1 = \arcsin\left[\frac{P}{B\cos\frac{2m\pi}{n}}\right] + \frac{2\pi m}{n} \tag{14.10a}$$

$$\theta_2 = -\arcsin\left[\frac{P}{B\cos\frac{2m\pi}{n}}\right] + \frac{2\pi m}{n}, \tag{14.10b}$$

and m is an integer such that

$$|m| \leq \lfloor \frac{n}{2\pi} \arccos\left(\sqrt{\frac{P}{B}}\right) \rfloor.$$

The total number of stable equilibria is given by

$$N_s = 1 + 2\lfloor \frac{n}{2\pi} \arccos\left(\sqrt{\frac{P}{B}}\right) \rfloor. \tag{14.11}$$

where $\lfloor x \rfloor$ denotes the floor value of x, that is, the largest integer value which is smaller than or equal to x. When $P = 0$, N_s reaches the upper bound derived in [13].

Remark 14.2 It can be seen from formula (14.11) that the number of the stable synchronous state increase linearly as the size n of the cycle increases. For the synchronous state with $m \neq 0$, power loop occurs in the cycle. For practical purposes the case $m = 0$ is desirable for transport of electricity, as in this case direct transport of power from the generator to the consumer is realized. Direct transport from generator to consumer minimizes energy losses that always accompany the transport of electrical power. Possible ways to avoid the clockwise-counterclockwise power loops is to control the power generation or loads, such that the phase angles are in the security range (14.19) which will be described in Sect. 14.4.

Besides these stable synchronous states, there may be more than 2^n synchronous states for the power network, which depends on the distribution of the power generation and loads and the topology, see [3, 8, 26, 30] for details. Because the unstable equilibrium points are on the potential energy boundary, it is important to find these equilibrium points for analyzing the nonlinear stability, detail will be further described in Sect. 14.5.

14.3.2 Braess' Paradox in Power Grids

A surprising finding in the synchronization of power grids is that adding more connections does not always improve the synchronization in the grid, but could also destroy an existing stable synchronized state.

A similar phenomenon was reported in the 1968 by Braess [5] in the context of traffic flow. It turned out that adding a new road to an existing traffic plan may sometimes lead to increased congestion of the traffic flow, in contrast to the expectation.

To illustrate how adding a new connection to a power grid can destroy the synchronization, we consider a configuration of a network consisting of 2 clusters of 4 nodes, which are coupled at the top and bottom nodes of each cluster; see Fig. 14.3. The same configuration was also considered in [52]. We assume each line to have the same capacity $B_{ij} = K$ for all $(i, j) \in \mathcal{E}$. The flow between nodes i and j is given by $F_{ij} = K \sin(\delta_i - \delta_j)$. For clarity, the consumer nodes with consumption P are depicted green and the generation nodes, with generation P, are blue. A straightforward study of this simple network, shows that an equilibrium configuration can be obtained when all blue nodes except the upper left one have phase $-\pi/2$ and all green nodes except the bottom right one have phase $\pi/2$. The upper left on lower right nodes both have phase 0. By taking the capacity of each line K to be equal to P, this configuration allows each line between a generator and a consumer to carry P units of power. Additionally, power P is transferred from the top right to the top left node as wel as from the bottom right to the bottom left node. We remark that this configuration is critical in the sense that a small increase in power generation or demand cannot be accommodated by the network.

When a connection between the upper left and lower right nodes is added, an overflow occurs, that is, the power flowing from the upper left node to the consumer nodes below is larger than the critical capacity K_c and therefore synchronization is lost. It has recently been shown that Braess' paradox can be prevented by using secondary control [48]. It turns out that all nodes need to be controlled, that is, both the generator and the consumer nodes, in order to prevent the Braess' paradox from happening. This demonstrates that the network topology is extremely important in order to guarantee reliable operation of the power grid, and that not only generator

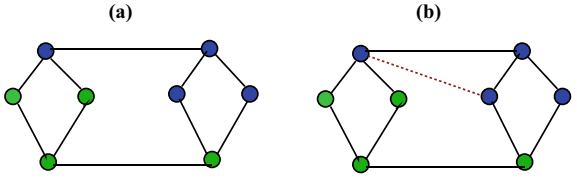

Fig. 14.3 A schematic of a simple network operating at critical capacity $K = K_c = P$. The system synchronizes in **a**, but adding a new connection shown in red between two generators induces an overload and destroys the synchronization of the system

nodes, but also consumer nodes should receive sufficient attention when introducing additional renewable power generators and consumers in the network.

Besides the work done on Braess' paradox in the group of Marc Timme [48, 52], a linear stability analysis has been carried out by Coletta and Jacquod [12] for simple linear chain networks. The work corroborates the results of Refs. [48, 52], by proving that for one-dimensional chain networks power can flow from consumer to generator and thereby surmounting the line capacity. This effect is equivalent to the Braess' paradox in a two-dimensional situation. Moreover, it was shown numerically that Braess' paradox can actually occur in real power grids, such as the UK power grid and the European Grid.

So far these calculations have all been carried out for purely capacitive networks, that is, without dissipative losses. As distributed generation of power is surging, dissipative effects will probably be more prevalent, which requires a more elaborate analysis including dissipative effects.

Remark 14.3 In the investigation of the Braess' Paradox in power grids, the existence condition of the synchronous state plays an important role such as in the finding and curing of it [48, 52]. Beside the critical line capacity K_c, the linear stability which will be discussed in Sect. 14.4 is also used as a stability metric in the study of the impact of the network topology[12, 52]. Possible ways to avoid the Braess' Paradox is to avoid the decrease of these metrics when adding new lines to the network. Control of power generation and loads is another way to curing this paradox.

14.4 Stability of the Linearized System

A non-linear system is linearly stable at an equilibrium state if the linearized system at that equilibrium state, determined by the Jacobian, is exponentially stable. The linear stability considers the local convergence speed at the neighborhood of the stable equilibrium point. This linear stability can be qualified by the real part of the eigenvalues. In this section, we introduce the linearization of the system and the dependence of the eigenvalues on the parameters of the power system. How to increase the linear stability by changing the parameters of the system will also be described.

Assume that there exists a synchronous state for the power system, which is denoted by $(\boldsymbol{\delta}^*, \mathbf{0})$. After linearization at the synchronous state, we derive

$$\dot{\boldsymbol{\delta}} = \boldsymbol{\omega}, \tag{14.12a}$$

$$\boldsymbol{M}\dot{\boldsymbol{\omega}} = -\boldsymbol{L}_c\boldsymbol{\delta} - \boldsymbol{D}\boldsymbol{\omega}. \tag{14.12b}$$

where $\boldsymbol{\delta} = \mathrm{col}(\delta_i) \in \mathbb{R}^n$, $\boldsymbol{\omega} = \mathrm{col}(\omega_i) \in \mathbb{R}^n$, $\boldsymbol{M} = \mathrm{diag}(M_i) \in \mathbb{R}^{n\times n}$, $\boldsymbol{L}_c = \big(B_{ij}\cos(\delta_i - \delta_j)\big) \in \mathbb{R}^{n\times n}$, $\boldsymbol{D} = \mathrm{diag}(D_i) \in \mathbb{R}^{n\times n}$. Here, $\mathrm{col}(\cdot)$ denotes a column vector and $\mathrm{diag}(\cdot)$ denotes a diagonal matrix.

In a power system, the *small signal stability* is the ability of the power system to maintain the synchronization when subjected to small disturbances. The behavior of the power system is best such that, after a small disturbance acting on the power system, the state of the system returns to the synchronous state. Preferably this return should be quickly. The small signal stability analysis is based on the linearization to provide valuable information about the characteristics of the system and help configure the corresponding parameters.

After linearizing the SMIB model (14.3) at an equilibrium point, we obtain

$$\dot{\delta} = \omega, \tag{14.13a}$$

$$M\dot{\omega} = -D\omega - \overline{B}\delta, \tag{14.13b}$$

where $\overline{B} = B\cos\delta_i^*$. The eigenvalues of the linear system can be calculated as

$$\lambda = \frac{-D \pm \sqrt{D^2 - 4\overline{B}}}{2} \tag{14.14}$$

from which it can be obtained that when $\overline{B} = B\cos\delta_0^* > 0$, all the eigenvalues have negative real part. Thus the system is stable at the equilibrium δ_0 according to the second Lyapunov method for determining the stability of a nonlinear system. However, with $\overline{B} = B\cos\delta_1^* < 0$, there is one eigenvalue which has positive real part. This means that the system is unstable at the equilibrium point δ_1^*. Hence, a security condition can be obtained for the stability of the equilibrium point as $\cos\delta^* > 0$, which can be further expressed as $-\frac{\pi}{2} < \delta^* < \frac{\pi}{2}$. For the SMIB model, it is obvious that there is only one stable equilibrium point in the security range of phase angle.

The linear stability analysis of the system (14.1) is much more complex than the SMIB mode because of the high dimension. The system (14.12) has $2n$ equations, and there are $2n$ eigenvalues which depend on $\boldsymbol{M}$, $\boldsymbol{L}_c$, $\boldsymbol{D}$. In practice, both $\boldsymbol{M}$ and $\boldsymbol{D}$ are positive definite for power systems. $\boldsymbol{L}_c$ involves the topology of the network and the line capacities. It has been proven in [57] that with positive definite $\boldsymbol{M}$ and $\boldsymbol{D}$ the sign of the real part of the eigenvalues depends on the eigenvalues of $\boldsymbol{L}_c$. This is explained as follows.

The system (14.12) can be written in the compact form

$$\begin{pmatrix} \dot{\boldsymbol{\delta}} \\ \dot{\boldsymbol{\omega}} \end{pmatrix} = \begin{pmatrix} \mathbf{0} & \boldsymbol{I} \\ -\boldsymbol{L_m} & \boldsymbol{\beta} \end{pmatrix} \begin{pmatrix} \boldsymbol{\delta} \\ \boldsymbol{\omega} \end{pmatrix} \tag{14.15}$$

where $\boldsymbol{L}_m = \boldsymbol{M}^{-1}\boldsymbol{L}_c, \boldsymbol{\beta} = \mathrm{diag}(D_i/M_i) \in \mathbb{R}^n$. We assume that all the components of $\boldsymbol{\beta}$ are identical, i.e., $\beta_i = \beta$. Let $\boldsymbol{Q} \in \mathbb{R}^{n\times n}$ be the matrix formed by the eigenvectors of $\boldsymbol{L}_m$ such that

$$\boldsymbol{Q}^{-1}\boldsymbol{L}_m\boldsymbol{Q} = \boldsymbol{\Lambda}$$

where $\boldsymbol{\Lambda}$ is a diagonal matrix with the diagonal component being the eigenvalues $0 = \lambda_1 < \lambda_2 \leq \lambda_2 \cdots \leq \lambda_n$ of $\boldsymbol{L}_m$ as its columns. Here all the eigenvalues of $\boldsymbol{L}_m$ are

real even though $\boldsymbol{L}_m$ is not symmetric [34]. Let $\boldsymbol{X}_1 = Q^{-1}\boldsymbol{\delta}$ and $\boldsymbol{X}_2 = Q^{-1}\boldsymbol{\omega}$. These formulas transform (14.15) to

$$\begin{pmatrix} \dot{\boldsymbol{X}}_1 \\ \dot{\boldsymbol{X}}_2 \end{pmatrix} = \begin{pmatrix} \mathbf{0} & \boldsymbol{I} \\ -\boldsymbol{\Lambda} & \boldsymbol{\beta} \end{pmatrix} \begin{pmatrix} \boldsymbol{X_1} \\ \boldsymbol{X_2} \end{pmatrix} \tag{14.16}$$

which consists of n decoupled sub-systems as follows

$$\begin{pmatrix} \dot{X}_{1i} \\ \dot{X}_{2i} \end{pmatrix} = \begin{pmatrix} 0 & 1 \\ -\lambda_i & \beta \end{pmatrix} \begin{pmatrix} X_{1i} \\ X_{2i} \end{pmatrix}, \ i = 1, \ldots, n. \tag{14.17}$$

Because the eigenvalue $\lambda_1 = 0$, we do not consider the subsystem $i = 1$ which in fact does not influence the synchronization due to the phase rotation. For the subsystems $i = 2, \cdots, n$, the eigenvalues of (14.12) can be calculated as follows

$$\alpha_{i\pm} = -\frac{\beta}{2} \pm \frac{1}{2}\sqrt{\beta^2 - 4\lambda_i}, \tag{14.18}$$

which has a similar form as the eigenvalues of the SMIB model in (14.14). It can be easily observed that with $\beta > 0$, the sign of the real part of α_i is determined by λ_i, and the synchronous state is Lyapunov stable if and only if λ_i is positive for $i = 2, \ldots, n$. Because $\boldsymbol{M}$ is a diagonal positive definite matrix which does not impact the non-negative definite of $\boldsymbol{L}_m$, the number of eigenvalues of L_m with a positive real part equals the number of eigenvalues of L_c with a positive real part. Thus, the synchronous state $(\boldsymbol{\delta}^*, \mathbf{0})$ is Lyapunov stable if and only if $\boldsymbol{L}_c$ is non-negative definite.

By Lyapunov stability theory, a synchronous state is unstable if there is an eigenvalue λ_i with strictly positive real part for the linearized system at this state. The unstable synchronous state is called of *type* j if the number of eigenvalues λ_i with strictly positive real-part is j. In other words, the dimension of the unstable manifold of the type j equilibrium point is j. It can be observed from (14.18) that if $\lambda_i < 0$, α_{i+} has a positive real part, then it will lead to an unstable manifold and that the number of the eigenvalues of the power network with positive real part equals that of the negative eigenvalues of $\boldsymbol{L}_m$. Because the number of the eigenvalues of $\boldsymbol{L}_m$ with positive real part equals to that of $\boldsymbol{L}_c$, the synchronous state $(\boldsymbol{\delta}^*, \mathbf{0})$ is of type j if $\boldsymbol{L}_c$ has j negative eigenvalues. This statement can be applied to the determination of type j equilibrium point of the power system with special topology, such as acyclic network and cyclic network, which will be further discussed in Sect. 14.5.

From the above discussions it is clear that the eigenvalues of the Laplacian matrix $\boldsymbol{L}_c$ play an important role in the stability analysis of power systems. It is well known that if the weights $B_{ij} \cos(\delta_i^* - \delta_j^*)$ for $(i, j) \in \mathcal{E}$ are positive, all the non-zero eigenvalues of $\boldsymbol{L}_c$ are positive. For the unstable synchronous state, there exist lines with negative weight. The characteristic of the eigenvalues of the Laplacian matrix of weighted network with *negative weight* has been investigated in [6], in which more details on the determination of the number of negative eigenvalues can be found.

Statement 14.1 For general configuration of $M_i > 0$ and $D_i > 0$ in the power system (14.1), it also holds that the synchronous state is stable if and only if all the non-zero eigenvalues of $\boldsymbol{L}_c$ are positive. Since $\boldsymbol{L}_c$ is the Laplacian matrix of the network with weight $B_{ij}\cos(\delta_i^* - \delta_j^*)$ for all the edge $(i, j) \in \mathcal{E}$, it can be derived that if all the weights are positive, $\boldsymbol{L}_c$ is non-negative definite. With $B_{ij}\cos(\delta_i^* - \delta_j^*) > 0$, the security condition for stability can be obtained

$$|\delta_i^* - \delta_j^*| < \frac{\pi}{2}, \ \forall (i, j) \in \mathcal{E}, \tag{14.19}$$

which is a well-known sufficient condition for the Lapunov stability of the synchronous state. □

For details of the proof of the above statement, we refer to [46, 57].

Statement 14.2 The synchronous state in this security range is unique and stable for the lossless power network. However, this is not true for lossy power networks, see [46] for details. □

The linear stability of the system is qualified by the absolute value of $\mathrm{Re}(\alpha_{i+})$ for $i = 2, \ldots, n$. Figure 14.4 illustrates how $\mathrm{Re}(\alpha_{i+})$ depends on β and α_i. For each subsystem described by (14.17), there is a minimum for $\mathrm{Re}(\alpha_{i+})$ with respect to β. This minimum value $\mathrm{Re}(\alpha_{i+}) = -\sqrt{\lambda_i}$ is obtained when setting $\beta = 2\sqrt{\lambda_i}$ in (14.18). If λ_i increases then the minimal value decreases, hence $\mathrm{Re}(\alpha_{i+})$ is limited by the second smallest eigenvalue λ_2 of $\boldsymbol{L}_m$. Thus, the optimal configuration of β can be obtained as

$$\beta_{\mathrm{opt}} = 2\sqrt{\lambda_2}. \tag{14.20}$$

From $\lambda_i > \lambda_2$ for $i = 3, \ldots, n$, it can be derived that if $\beta = \beta_{\mathrm{opt}}$, the real-part of all the eigenvalues of (14.12) are all identical, i.e.,

$$\mathrm{Re}(\alpha_{i+}) = \frac{\beta_{\mathrm{opt}}}{2}, \ i = 2, \ldots, n.$$

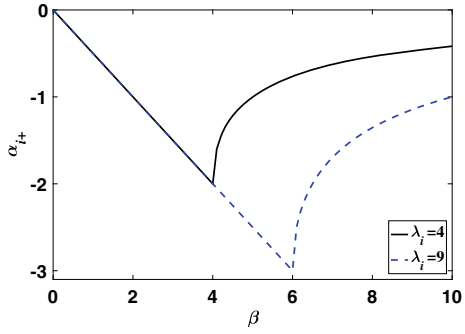

Fig. 14.4 The real part of α_{i+} with respect to β and λ_i

If β is smaller than β_{opt}, the real part $\text{Re}(\alpha_i+)$ can be increased by increasing the damping coefficient as $D_i = \beta M_i$ due to the independence of $\boldsymbol{L}_m$ on D_i, and the optimal configuration is $D_i = 2\sqrt{\lambda_2}/M_i$.

Statement 14.3 Since $\boldsymbol{L}_m = \boldsymbol{M}^{-1}\boldsymbol{L}_c$, then the eigenvalue λ_2 of $\boldsymbol{L}_m$ increases if the eigenvalues of $\boldsymbol{L}_c$ increase. Due to the fact that $\boldsymbol{L}_c$ is determined by the synchronous state, the topology and the capacity of transmission lines, the linear stability of the power system can be improved by controlling the power injection, well-designed topology and replacement of the transmission lines with low capacity by those with high capacity. Once these parameters are determined, the damping coefficient D_i can be determined by $D_i = 2\sqrt{\lambda_2}M_i$. □

Algorithms for maxmizing the second smallest eigenvalues by determining the state have been investigated in [21] which can be referred to for details.

Statement 14.4 The optimal configuration $\beta = \beta_{\text{opt}}$ is formulated with the assumption that all the components of $\boldsymbol{\beta}$ are identical. It has been shown that for non-identical β_i this setting is optimal along any given direction in the β_i-space for many power systems [34, 35]. Hence, this configuration and increasing the second smallest eigenvalue is appropriate for enhancing the stability. For details of the analysis, we refer to [34, 35]. □

The impact of the Braess' paradox on the linear stability has been investigated in [12], in which it is shown that adding a line to the network may decrease the linear stability of a power network. The linear stability of cyclic power network has been studied in [55]. An analytic formula of the eigenvalues of the linearized system is obtained, which demonstrated that the linear stability decreases as the size of the network increases. Simulations with various networks showed that the linear stability decreases as the heterogeneity of the power injection increases. In other words, the linear stability can be increased by reducing the heterogeneity of the power injection (loads).

14.5 The Nonlinear Stability

In this section, we introduce the synchronization stability of power systems. The stability region of power systems has been analyzed by Chiang et al. [11] and Zaborszky et al. [58]. However, because of the large-scale and complexity of the power network, the basin of attraction, related to transient stability, has a high computational complexity for numerical approximation. In this section, we introduce the *energy barrier* which is a conservative estimate of the stability margin of the power system.

Inspired by the *direct method* to estimate whether the power system is stable after a disturbance [10, 23, 24, 51], we explain how we can use the energy barrier method to determine the transient stability in the case of the SMIB model.

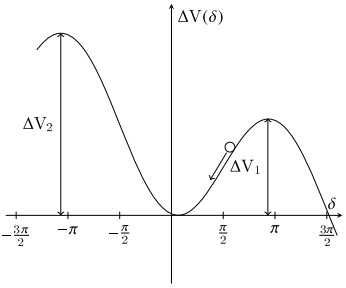

Fig. 14.5 The potential energy landscape of the SMIB system

The potential energy of this system is

$$\mathrm{V}(\delta) = -B\cos\delta - P\delta.$$

Figure 14.5b plots the potential energy difference $\mathrm{V}(\delta) - \mathrm{V}(\delta_0)$ where $\delta_0 = \arcsin P/B$ is the phase angle difference at the steady state. In the figure, the position and the speed of the ball displayed are δ and ω respectively. The potential energy possesses three extreme points in the range $(-3\pi/2, 3\pi/2)$, which include two unstable equilibria and one stable equilibrium. It can be observed that the trajectory will converge to the minimum of $\mathrm{V}(\delta)$ if its kinetic energy is smaller than the potential energy $\Delta\mathrm{V}_1$ and $\Delta\mathrm{V}_2$. If obtaining enough energy from a disturbance to overcome the potential energy, the trajectory will escape from the valley and thus the system desynchronizes. Hence, the energy barrier $\Delta\mathrm{V}_1$ and $\Delta\mathrm{V}_2$ which are the potential energy differences between the two unstable equilibria and the stable equilibrium, can be used to measure the synchronization stability, which have the following formula [10]

$$\Delta\mathrm{V}_1 = P(-\pi + 2\arcsin\frac{P}{B}) + 2\sqrt{B^2 - P^2}, \tag{14.21a}$$

$$\Delta\mathrm{V}_2 = P(\pi + 2\arcsin\frac{P}{B}) + 2\sqrt{B^2 - P^2}. \tag{14.21b}$$

From the above equations it is immediately clear that $\Delta\mathrm{V}_1$ decreases while $\Delta\mathrm{V}_2$ increases as the transmitted power P increases. As shown in Fig. 14.5b, it is much easier for the trajectory to overcome $\Delta\mathrm{V}_1$ to escape from the valley than $\Delta\mathrm{V}_2$. So $\Delta\mathrm{V}_1$ provides a conservative approximation of the basin of attraction and can be used to measure the transient stability.

For the power network (14.1), the calculation of the energy barrier is far more complex. The potential energy $V(\boldsymbol{\delta})$ is defined as

$$V(\boldsymbol{\delta}) = -B\sum_{(i,j)\in\mathcal{E}}\cos(\delta_i - \delta_j) - \sum_{i=1}^{N} P_i\delta_i. \tag{14.22}$$

The primary idea behind estimating the region of attraction of a stable equilibrium by the direct method, is that this region is bounded by a manifold $\mathcal{M}$ of the type-1 equilibria that reside on the potential energy boundary surface (PEBS) of the stable equilibrium. The PEBS can be viewed as the stability boundary of the associated gradient system [10, 51]

$$\frac{d\delta_i}{dt} = -\frac{\partial V(\boldsymbol{\delta})}{\partial \delta_i}. \tag{14.23}$$

The *closest equilibrium* is defined as the one with the lowest potential energy on the PEBS. By calculating the closest equilibrium with potential energy $V_{\min}$ and equating this to the total energy, it is guaranteed that points within the region bounded by the manifold $\mathcal{M} = \{(\delta, \omega) | E(\delta, \omega) = V_{\min}\}$, will always converge to the stable equilibrium point contained in $\mathcal{M}$. Various algorithms for the calculation of the closest equilibrium points are proposed, see [23, 24].

The idea of estimating the region of stability by type-1 equilibria is probably best illustrated by considering a simple example of a three-node network depicted in Fig. 14.6a. The 6 unstable equilibria are local minima on the potential energy boundary surface (PEBS) plotted by the black dash-dotted line. These minima are all type-1. The equilibrium 1 and 4, 2 and 5, 3 and 6 are caused by θ_1, θ_2 and θ_3 exceeding $\pi/2$ respectively. Because equilibrium point 1 has the smallest energy, it is the closest equilibrium point on the PEBS.

A small perturbation in the direction to saddle point 1, depicted by the red dashed curve leads to desynchronization, whereas a larger perturbation in a different direction (blue solid curve) eventually decays toward the stable equilibrium point and hence the system stays synchronized. This shows the conservativity of the direct method and the challenges in calculating the region of stability, as it depends on both the direction and size of the perturbation. One approach to this problem is to determine the so-

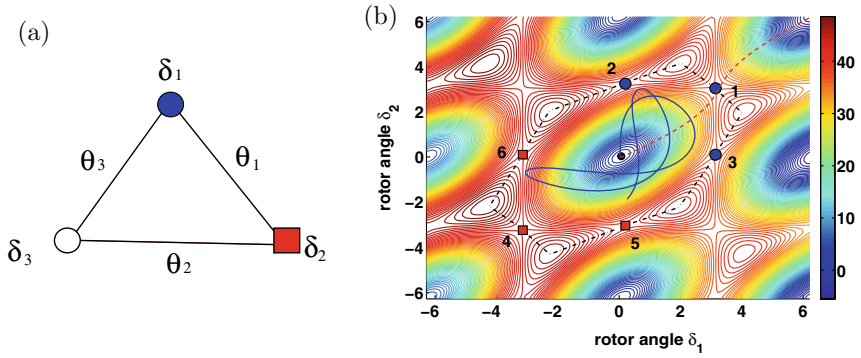

Fig. 14.6 **a** The 3-node power grid. **b** The potential energy of the three nodes power grid as a function of δ_i where $P_1/K = 0.125$, $P_2/K = -0.125$, and $P_3/K = 0$

called *controlling unstable equilibrium point*, which was developed. The method is not considered in this paper and we focus on the energy barrier, see [7, 11, 49]

It is obvious that if the potential energy of the type-1 equilibrium point is larger, the system can stand more serious disturbances. Hence the potential energy of all the type-1 equilibrium points can be used to measure the transient stability. However, to calculate the energy barrier, it is necessary to find all the type-1 equilibria which is actually a NP hard problem for a general network with many cycles. This idea is applied to a cyclic power network to investigate the impact of the cycles on the transient stability by the authors [55].

We focus on the stable equilibrium point with power flows in all the lines being P and the phase angle differences being $\arcsin P/B$, which is the same as in the SMIB model.

For this cyclic network, similar as in the SMIB model, the energy barrier can be calculated as

$$\Delta V_I^c = P\left(-\pi + 2\arcsin\frac{P}{B}\right) + 2B\sqrt{1-\frac{P^2}{B^2}} + \Delta U_I, \tag{14.24a}$$

$$\Delta U_I = \frac{2B}{n}\left(\frac{\pi}{2} - \arcsin\frac{P}{B}\right)^2\sqrt{1-\frac{P^2}{B^2}} + O\left(n^{-2}\right). \tag{14.24b}$$

This energy is a conservative approximation of the minimum energy from the disturbance that destroys the stability. When the system loses synchronization, there must be a line in which the phase angle difference is larger than $\pi/2$. When comparing this energy with that of the SMIB model in (14.21b), it can be found that ΔV_I^c is larger than ΔV_1. The minimum energy that leads to phase angle differences in branch lines exceeding $\pi/2$, are the same as ΔV_1 when the power transmission is P. Thus, the lines in a cycle are stronger than a branch line when they transfer the same amount of power. This explains in a micro-perceptive why dead-ends in a network undermine the stability.

Statement 14.5 With this finding, The stability of a nonlinear power system can be improved by either forming small cycles in the power network or by control so that the power-line branches transfer less power than the power lines in the cycles. □

From the comparison, it can also be deduced that the phase angle differences of the lines in cycles can be larger than those of lines which are not in cycles. In other words, with the same line capacity, the lines in cycles can transmit more power than those that are not in cycles.

Remark 14.4 However, this energy barrier focus on the potential energy landscape, in which the impact of the inertia and damping coefficients on the stability are not considered. This makes the energy barrier very conservative for the estimation of stability margin. In addition, for the large scale power networks with complex topology, finding all the type-1 equilibrium points is a challenging numerical problem due to the exponentially increase of the number of equilibrium points with the size of the network.

14.6 Conclusion

In this chapter, stability metrics and corresponding strategies to improve the stability of non-linear power systems have been introduced. The controllable factors that impact the stability include the inertia of synchronous machines, the damping coefficients, the topology of the network which involves the line capacity and the power generation and loads.

From the existence condition of the synchronous state, stability metric K_c can be extracted for the synchronization stability improvement by changing the topology of the network, the power generation and loads. Because this metric focuses on the synchronous state, the impact of the inertia of the synchronous machines and the damping coefficients are not reflected by this metric. Due to the equivalence between the power system and the Kuramoto model, the result obtained from the study of the existence of the Kuramoto model can be applied to the power system.

If a synchronous state exists for a power network, its local stability can be determined by the small signal stability based on the Lyapunov method. The stability of the linearized system is measured by the absolute value of the real part of the eigenvalues. With the optimal configuration method of $\beta_i = \beta_{\text{opt}}$, the linear stability can be enhanced by changing all the four factors. Note that it is demonstrated in [35] that the point with this setting in the $\boldsymbol{\beta}$-space is not a true local optimum for the linear stability. The method to find the optimum of the linear stability still needs further investigation. In addition, the linear stability formalism can only explore the local landscape of the stability region.

The energy barrier for the stability margin estimation is inspired by the direct method for the estimation of the system after a disturbance. It has been found that forming small cycles can increasing the stability margin. However, similar as the basin stability, this energy barrier is hard to be applied as a stability metric that can be used to form an optimization framework. In addition, the energy barrier focuses on the potential energy of the power network, it only reflects the impact of the topology and the power generation and loads on the stability.

The stability of the power network can be improved via various strategies. However, it is obvious that the optimal solution from these metrics are non-identical due to that none of them can includes all the influential factors of the stability. How these solution related to the stability region and what are the relationship between these solutions still need further study.

References

1. Anderson, P.M., Fouad, A.A.: Power System Control and Stability. Wiley-IEEE Press (2002)
2. Arenas, A., Díaz-Guilera, A., Kurths, J., Moreno, Y., Zhou, C.: Synchronization in complex networks. Phys. Rep. **469**(3), 93–153 (2008)
3. Baillieul, J., Byrnes, C.: Geometric critical point analysis of lossless power system models. IEEE Trans. Circuits Syst. **29**(11), 724–737 (1982)

4. Bergen, A.R., Hill, D.J.: A structure preserving model for power system stability analysis. IEEE Trans. Power App. Syst. **1**, 25–35 (1981)
5. Braess, D.: Uber ein paradoxon aus der verkehrsplanung. Unternehmensforschung Operations Research **12** (1968)
6. Bronski, J.C., DeVille, L.: Spectral theory for dynamics on graphs containing attractive and repulsive interactions. SIAM J. Appl. Math. **74**(1), 83–105 (2014)
7. Chang, H.D., Chu, C.C., Cauley, G.: Direct stability analysis of electric power systems using energy functions: theory, applications, and perspective. Proc. IEEE **83**(11), 1497–1529 (1995)
8. Chen, T., Davis, R., Mehta, D.: Counting equilibria of the kuramoto model using birationally invariant intersection index. SIAM J. Appl. Algebra Geometry **2**(4), 489–507 (2018)
9. Chiang, H.D., Chu, C.C.: Theoretical foundation of the BCU method for direct stability analysis of network-reduction power system. Models with small transfer conductances. IEEE Trans. Circuits Syst. I. Fundam. Theory Appl. **42**(5), 252–265 (1995)
10. Chiang, H.D., Wu, F.F., Varaiya, P.P.: Foundations of the potential energy boundary surface method for power system transient stability analysis. IEEE Trans. Circuits Syst. **35**(6), 712–728 (1988)
11. Chiang, H.D., Hirsch, M.W., Wu, F.F.: Stability regions of nonlinear autonomous dynamical systems. IEEE Trans. Autom. Control **33**(1), 16–27 (1988)
12. Coletta, T., Jacquod, P.: Linear stability and the Braess paradox in coupled-oscillator networks and electric power grids. Phys. Rev. E **93**(3), 032222 (2016)
13. Delabays, R., Coletta, T., Jacquod, P.: Multistability of phase-locking and topological winding numbers in locally coupled kuramoto models on single-loop networks. J. Math. Phys. **57**(3) (2016)
14. Dörfler, F., Bullo, F.: On the critical coupling for kuramoto oscillators. SIAM J. Appl. Dynam. Syst. **10**(3), 1070–1099 (2011)
15. Dörfler, F., Bullo, F.: Synchronization in complex networks of phase oscillators: a survey. Automatica **50**(6), 1539–1564 (2014)
16. Dörfler, F., Simpson-Porco, J.W., Bullo, F.: Breaking the hierarchy: distributed control and economic optimality in microgrids. IEEE Trans. Control Netw. Syst. **3**(3), 241–253 (2016)
17. Hasler, M., Wang, C., Ilic, M., Zobian, A.: Computation of static stability margins in power systems using monotonicity. In: 1993 IEEE International Symposium on Circuits and Systems, vol. 4, pp. 2196–2199, May 1993
18. Ilić, M.D., Zaborszky, J.: Dynamics and Control of Large Electric Power Systems. Wiley (2000)
19. Khalil, H.K.: Nonlinear Systems, 3rd edn. Prentice Hall, Upper Saddle River, New Jersey 07458 (2002)
20. Khayat, Y., Shafiee, Q., Heydari, R., Naderi, M., Dragicevic, T., Simpson-Porco, J.W., Dorfler, F., Fathi, M., Blaabjerg, F., Guerrero, J.M., Bevrani, H.: On the secondary control architectures of ac microgrids: an overview. IEEE Trans. Power Electron. 1–1 (2019)
21. Kim, Y., Mesbahi, M.: On maximizing the second smallest eigenvalue of a state-dependent graph laplacian. IEEE Trans. Autom. Control **51**(1), 116–120 (2006)
22. Kundur, P.: Power System Stability and Control. McGraw-Hill (1994)
23. Lee, J., Chiang, H.D.: A singular fixed-point homotopy method to locate the closest unstable equilibrium point for transient stability region estimate. IEEE Trans. Circuits Syst. II, Exp. Briefs **51**(4), 185–189 (2004)
24. Liu, C.W., Thorp, J.S.: A novel method to compute the closest unstable equilibrium point for transient stability region estimate in power systems. IEEE Trans. Circuits Syst. I, Fundam. Theory Appl. **44**(7), 630–635 (1997)
25. Lozano, S., Buzna, L., Díaz-Guilera, A.: Role of network topology in the synchronization of power systems. Eur. Phys. J. B **85**(7), 231 (2012)
26. Luxemburg, L.A., Huang, G.: On the number of unstable equilibria of a class of nonlinear systems. In: 26th IEEE Conference Decision Control, vol. 20, pp. 889–894. IEEE (1987)
27. Manik, D., Timme, M., Witthaut, D.: Cycle flows and multistability in oscillatory networks. Chaos **27**(8), 083123 (2017)
28. Marris, E.: Energy: upgrading the grid. Nature **454**, 570–573 (2008)

29. Mehta, D., Daleo, N.S., Dörfler, F., Hauenstein, J.D.: Algebraic geometrization of the Kuramoto model: equilibria and stability analysis. Chaos **25**(5), 053103 (2015)
30. Mehta, D., Nguyen, H.D., Turitsyn, K.: Numerical polynomial homotopy continuation method to locate all the power flow solutions. IET Gener. Transm. Distrib. **10**(12), 2972–2980 (2016)
31. Menck, P.J., Heitzig, J., Kurths, J., Schellnhuber, H.J.: How dead ends undermine power grid stability. Nat. Commun. **5**, 3969 (2014)
32. Menck, P.J., Heitzig, J., Marwan, N., Kurths, J.: How basin stability complements the linear-stability paradigm. Nat. Phys. **9**(2), 89–92 (2013)
33. Milano, F.: Power Systems Analysis Toolbox. University of Castilla, Castilla-La Mancha, Spain (2008)
34. Motter, A.E., Myers, S.A., Anghel, M., Nishikawa, T.: Spontaneous synchrony in power-grid networks. Nat. Phys. **9**(3), 191–197 (2013)
35. Nishikawa, T., Molnar, F., Motter, A.E.: Stability landscape of power-grid synchronization. IFAC-PapersOnLine **48**(18), 1–6 (2015). 4th IFAC Conference on Analysis and Control of Chaotic Systems CHAOS 2015
36. Nishikawa, T., Motter, A.E.: Comparative analysis of existing models for power-grid synchronization. New J. Phys. **17**(1), 015012 (2015)
37. Nusse, H.E., Yorke, J.A.: Basins of attraction. Science **271**(5254), 1376–1380 (1996)
38. Ochab, J., Góra, P.F.: Synchronization of coupled oscillators in a local one-dimensional Kuramoto model. Acta. Phys. Pol. B Proc. Suppl. **3**, 453–462 (2010)
39. Pecora, L.M., Carroll, T.L.: Master stability functions for synchronized coupled systems. Phys. Rev. Lett. **80**(10), 2109–2112 (1998)
40. Rogge, J.A., Aeyels, D.: Stability of phase locking in a ring of unidirectionally coupled oscillators. J. Phys. A Math. Gen. **37**(46), 11135–11148 (2004)
41. Rohden, M., Sorge, A., Witthaut, D., Timme, M.: Impact of network topology on synchrony of oscillatory power grids. Chaos **24**(1), 013123 (2014)
42. Schavemaker, P., van der Sluis, L.: Electrical Power System Essentials. Wiley (2008)
43. Schiffer, J., Goldin, D., Raisch, J., Sezi, T.: Synchronization of droop-controlled microgrids with distributed rotational and electronic generation. In: 52nd IEEE Conference Decision and Control, pp. 2334–2339, Dec 2013
44. Schiffer, J., Ortega, R., Astolfi, A., Raisch, J., Sezi, T.: Conditions for stability of droop-controlled inverter-based microgrids. Automatica **50**(10), 2457–2469 (2014)
45. Simpson-Porco, J.W., Dörfler, F., Bullo, F.: Voltage collapse in complex power grids. Nat. Commun. **7**, 10790 (2016)
46. Skar, S.J.: Stability of multi-machine power systems with nontrivial transfer conductances. SIAM J. Appl. Math. **39**(3), 475–491 (1980)
47. Skardal, P.S., Taylor, D., Sun, J.: Optimal synchronization of complex networks. Phys. Rev. Lett. **113**(14), 144101 (2014)
48. Tchuisseu, E.B.T., Gomila, D., Colet, P., Witthaut, D., Timme, M., Schäfer, B.: Curing braess' paradox by secondary control in power grids. New J. Phys. **20**(8), 083005 (2018)
49. Treinen, R.T., Vittal, V., Kliemann, W.: An improved technique to determine the controlling unstable equilibrium point in a power system. IEEE Trans. Circuits Syst. I, Fundam. Theory Appl. **43**(4), 313–323 (1996)
50. Van Mieghem, P.: Graph Spectra of Complex Networks. Cambridge University Press (2008)
51. Varaiya, P.P., Wu, F.F., Chen, R.L.: Direct methods for transient stability analysis of power systems: recent results. Proc. IEEE **73**(12), 1703–1715 (1985)
52. Witthaut, D., Timme, Marc: Braess's paradox in oscillator networks, desynchronization and power outage. New J. Phys. **14**(8), 083036 (2012)
53. Wood, A.J., Wollenberg, B.F., Sheble, G.B.: Power Generation, Operation, and Control, 3rd edn. Wiley-IEEE, Hoboken, New Jersey (2013)
54. Xi, K., Lin, H.X., Shen, C., van Schuppen, J.H.: Multi-level power-imbalance allocation control for secondary frequency control of power systems. IEEE Trans. Autom. Control, pp 1 (2019)
55. Xi, K., Dubbeldam, J.L.A., Lin, H.X.: Synchronization of cyclic power grids: equilibria and stability of the synchronous state. Chaos **27**(1), 013109 (2017)

56. Xi, K., Dubbeldam, J.L.A., Lin, H.X., van Schuppen, J.H.: Power imbalance allocation control of power systems-secondary frequency control. Automatica **92**, 72–85 (2018)
57. Zaborsky, J., Huang, G., Leung, T.C., Zheng, B.: Stability monitoring on the large electric power system. In: 24th IEEE Conference Decision Control, vol. 24, pp. 787–798. IEEE (1985)
58. Zaborszky, J., Huang, G., Zheng, B., Leung, T.C.: On the phase portrait of a class of large nonlinear dynamic systems such as the power system. IEEE Trans. Autom. Control **33**(1), 4–15 (1988)